

A tunable heat pump by modulating the coupling to the leads

Eduardo C. Cuansing and Jian-Sheng Wang

*Department of Physics and Centre for Computational Science and Engineering,
National University of Singapore, Singapore 117542, Republic of Singapore*

(Dated: May 27, 2010)

We follow the nonequilibrium Green's function formalism to study time-dependent thermal transport in a linear chain system consisting of two semi-infinite leads connected together by a coupling that is harmonically modulated in time. The modulation is driven by an external agent that can absorb and emit energy. We determine the energy current flowing out of the leads exactly by solving numerically the Dyson equation for the contour-ordered Green's function. The amplitude of the modulated coupling is of the same order as the interparticle coupling within each lead. When the leads have the same temperature, our numerical results show that modulating the coupling between the leads may direct energy to either flow into the leads simultaneously or flow out of the leads simultaneously, depending on the values of the driving frequency and temperature. A special combination of values of the driving frequency and temperature exists wherein no net energy flows into or out of the leads, even for long times. When one of the leads is warmer than the other, net energy flows out of the warmer lead. For the cooler lead, however, the direction of the energy current flow depends on the values of the driving frequency and temperature. In addition, we find transient effects to become more pronounced for higher values of the driving frequency.

PACS numbers: 44.10.+i, 63.22.-m, 66.70.Lm

I. INTRODUCTION

The transport of phonons in mesoscale and nanoscale devices is an important issue relevant to the questions of heat generation in devices and their structural stability. Experiments measuring the heat generated in electric current-carrying metal-molecule junctions found that the generated heat can be substantial [1] and can therefore threaten the device's integrity. Efficiently dissipating heat in such devices is thus important and a problem that must be considered. A way of manipulating heat in nanoscale devices is by utilizing a heat pump that directs heat from one part of the device to another or to an external reservoir by means of an applied external work. Models on the mechanism of such a nanoscale heat pump have been proposed in systems where the pump works against the thermal gradient between two reservoirs in the system [2–4] and in systems where there is no net thermal bias between the two reservoirs [5–7]. In addition, other models employing quantum particle pumps that differentiate and filter hot and cold particles have been proposed [8]. In this paper we present an alternative model of a phonon pump that directs energy, and thus heat, into or out of regions of the device by dynamically modulating the coupling between those regions. The model is different from previous models of heat pumps where requirements of either modulating the temperatures of reservoirs [6, 7], or having an external driving force acting at the central portion of the device [3–5], or filtering particles according to their temperatures [2, 8] should be satisfied. Our model, in comparison, requires an external agent that can either absorb or release heat and is dynamically modulating the coupling between two parts of the device. A thermal gradient is not necessary for our model phonon pump to work.

To induce a phonon pump action in our model the coupling between the two parts of the system is harmonically modulated in time. Experimentally, this can be done by, for example, harmonically varying the distance between two molecules, therefore modulating the coupling between the molecules. Time-dependent transport of phonons in molecular systems, however, is a topic that is not yet fully understood theoretically. Although our understanding of the subject has improved tremendously during the past few years, most of the results pertain to steady-state and long-time behavior [9]. Time-dependent phonon transport with non-adiabatic and strong perturbations has recently been studied in a thermal switch device where the coupling to the reservoirs is abruptly turned on [10]. In this paper we extend the thermal switch model to one where the reservoir coupling is modulated in time. The system subsequently acts as a phonon pump that can be tuned by varying the frequency of modulation of the coupling to the reservoirs.

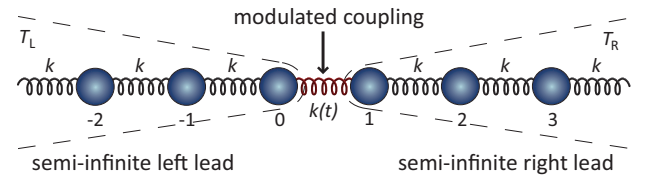


FIG. 1: (Color online) An illustration of an infinite linear chain whose two semi-infinite parts are connected by a coupling $k(t)$ that is modulated in time. The labels of the first three particles in each lead are shown beside each particle. Nearest-neighbor particles within the leads interact via an interparticle spring constant k . An on-site spring with spring constant k_0 is also experienced by each particle.

II. MODEL AND THEORETICAL APPROACH

In this paper we consider phonon transport in a one-dimensional chain. Shown in Fig. 1 is a linear chain consisting of two semi-infinite leads, or reservoirs, coupled together by a coupling $k(t)$ that is modulated in time. The particles in each lead are coupled to their nearest neighbors by a coupling constant k . In addition, each particle experiences an on-site potential with spring constant k_0 . The temperatures in the left and right leads are T_L and T_R , respectively. The particles can vibrate only along the horizontal axis. Particles in each lead follow a Hamiltonian with purely harmonic, nearest-neighbor, interactions that do not vary in time:

$$H^\alpha = \frac{1}{2} \sum_i (\dot{u}_i^\alpha)^2 + \frac{1}{2} \sum_{ij} u_i^\alpha K_{ij}^\alpha u_j^\alpha, \quad \alpha = L, R, \quad (1)$$

where the first sum is over all particles and the second sum is over all nearest-neighbor pairs in the leads. Each nearest-neighbor pair, however, is considered twice and so we divide the second term by two. The transformed coordinates $u_i = \sqrt{m}x_i$ is used, where x_i is the relative displacement of the i -th particle of mass m , and \mathbf{K}^α is the coupling matrix. This matrix is from the dynamic matrix of the full system:

$$\mathbf{K} = \begin{pmatrix} \mathbf{K}^L & \mathbf{V}^{LR} \\ \mathbf{V}^{RL} & \mathbf{K}^R \end{pmatrix}, \quad (2)$$

where in the one-dimensional chain the spring constant matrices \mathbf{K}^L and \mathbf{K}^R are semi-infinite tridiagonal submatrices consisting of $2k + k_0$ along the diagonal and $-k$ along both off-diagonals. The coupling matrices $\mathbf{V}^{LR}(t)$ and $\mathbf{V}^{RL}(t)$ are the couplings to the leads that vary in time. The Hamiltonian involving the lead coupling is:

$$H^{LR}(t) = \sum_{ij} u_i^L V_{ij}^{LR}(t) u_j^R, \quad (3)$$

where the sum is over all particles in each lead that are directly coupled to the other lead. For the linear chain shown in Fig. 1 the coupling matrices each have only one nonzero element:

$$V_{01}^{LR}(t) = -k(t) \quad \text{and} \quad V_{10}^{RL}(t) = -k(t). \quad (4)$$

Notice that during the same instant in time, $H^{LR}(t) = H^{RL}(t)$. The total time-dependent Hamiltonian for the two-lead system is

$$H(t) = H^L + H^R + H^{LR}(t). \quad (5)$$

Note that what we have is an open system consisting of the two leads and their coupling that is being modulated by an external agent. The energy, therefore, that this two-lead system gains or loses is coming from or going to the external agent.

The energy current flowing out of the left lead is

$$I^L(t) = - \left\langle \frac{dH^L}{dt} \right\rangle = \frac{i}{\hbar} \langle [H^L, H] \rangle, \quad (6)$$

i.e., it is the negative of the expectation value of the rate of change in H^L . The Heisenberg equation of motion is used in the second equality. The position and momentum of a particle obey the commutation relation

$$[u_i^\alpha(t), \dot{u}_j^\beta(t)] = i\hbar \delta_{ij} \delta^{\alpha\beta}, \quad \alpha, \beta = L, R, \quad (7)$$

where i and j are particle labels. Note that this commutation relation only exists at the same instant in time. We thus find that the only term in H that does not commute with H^L is H^{LR} . Equation (6) therefore becomes

$$I^L(t) = \frac{i}{2\hbar} \sum_{jmn} \langle [\dot{u}_j^L \dot{u}_j^L, u_m^L V_{mn}^{LR} u_n^R] \rangle, \quad (8)$$

where all the terms in the right-hand side occur at the same time t . Now define the real-time lesser Green's function as

$$G_{ij}^{RL,<}(t_1, t_2) = -\frac{i}{\hbar} \langle u_j^L(t_2) u_i^R(t_1) \rangle. \quad (9)$$

We would like to use this Green's function to properly calculate the current. Re-expressing Eq. (8) using two time variables we get

$$I^L(t) = \frac{i}{2\hbar} \sum_{jmn} \langle [\dot{u}_j^L(t_2) \dot{u}_j^L(t_2), u_m^L(t_1) V_{mn}^{LR}(t_1) u_n^R(t_1)] \rangle \Big|_{t_1=t_2=t}, \quad (10)$$

where we set $t_1 = t_2 = t$ in the end. Since $V^{LR}(t) = V^{RL}(t)$, we have

$$I^L(t) = \frac{i}{2\hbar} \sum_{jmn} c_{jm}(t_2, t_1) V_{mn}^{LR}(t_1) \frac{\partial}{\partial t_2} \{ \langle u_j^L(t_2) u_n^R(t_1) \rangle + \langle u_n^R(t_1) u_j^L(t_2) \rangle \} \Big|_{t_1=t_2=t}, \quad (11)$$

where $c_{jm}(t_2, t_1) = [\dot{u}_j^L(t_2), u_m^L(t_1)]$. Making use of the lesser Green's function, Eq. (9), and its complex conjugate, we get

$$I^L(t) = -i \sum_{jmn} c_{jm}(t_2, t_1) V_{mn}^{LR}(t_1) \times \text{Im} \left\{ \frac{\partial}{\partial t_2} G_{nj}^{RL,<}(t_1, t_2) \right\} \Big|_{t_1=t_2=t}, \quad (12)$$

where “Im” means taking the imaginary part. Equation (12) is a general equation for the energy current flowing out of the left lead. Note that the result is independent of the dimension of the system. For the one-dimensional linear chain setup shown in Fig. 1 we use Eq. (4) and the fact that $c_{jm}(t, t) = -i\hbar \delta_{jm}$ to get

$$I^L(t) = \hbar k(t) \text{Im} \left\{ \frac{\partial}{\partial t_2} G_{10}^{RL,<}(t_1, t_2) \right\} \Big|_{t_1=t_2=t}. \quad (13)$$

Equation (13) is the primary equation we use to calculate the current flowing out of the left lead. Similarly, we

define the energy current flowing out of the right lead as $I^R(t) = -\langle dH^R/dt \rangle$ and derive an expression in terms of the lesser Green's function:

$$I^R(t) = \hbar k(t) \text{Im} \left\{ \frac{\partial}{\partial t_2} G_{01}^{\text{LR},<}(t_1, t_2) \right\} \Big|_{t_1=t_2=t}. \quad (14)$$

To calculate the currents in Eqs. (13) and (14) we need to determine the nonequilibrium lesser Green's functions in those equations. We now follow the Schwinger-Keldysh formalism, in which a complex-time contour is employed [11–14], to determine the Green's functions.

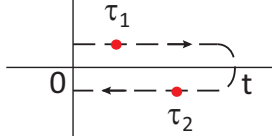


FIG. 2: The complex-time contour in the Keldysh formalism. The path of the contour begins at time $t = 0$, goes to time t , and then goes back to time $t = 0$. τ_1 and τ_2 are complex-time variables along the contour.

Shown in Fig. 2 is the Keldysh contour we use. At times $t < 0$ we consider the left and right leads to be decoupled and each is in thermal equilibrium with temperature T_L and T_R , respectively. At time $t = 0$ the coupling between the leads, $k(t)$, is switched on. We then calculate the energy current at time t , i.e., the time at the right edge of the contour. Note that instead of

adiabatic switch-on, the coupling $k(t)$ is abruptly turned on at $t = 0$. In addition, the left and right leads are uncorrelated before $t = 0$ and so there is no imaginary tail when the contour goes back to time $t = 0$. We now define the contour-ordered Green's function

$$G_{ij}^{\text{RL}}(\tau_1, \tau_2) = -\frac{i}{\hbar} \langle T_c u_i^R(\tau_1) u_j^L(\tau_2) \rangle, \quad (15)$$

where the T_c is the contour-ordering operator, τ_1 and τ_2 are contour variables, and u_i^R and u_j^L are operators in the Heisenberg picture. Transforming to the interaction picture, we separate the Hamiltonian in Eq. (5) into the free-particle quadratic part, $H_0 = H^L + H^R$, and the interaction part, $H_{\text{int}}(t) = H^{\text{LR}}(t)$. We then write the contour-ordered Green's function in the interaction picture as

$$G_{ij}^{\text{RL}}(\tau_1, \tau_2) = -\frac{i}{\hbar} \left\langle T_c e^{-i/\hbar \int_c H_{\text{int}}(\tau') d\tau'} u_i^R(\tau_1) u_j^L(\tau_2) \right\rangle, \quad (16)$$

where c is the contour shown in Fig. 2 and the average is now taken with respect to the equilibrium distributions when $t < 0$. We expand the exponential to perform a perturbation expansion. For the 0th-order term we find

$$G_{ij,0}^{\text{RL}}(\tau_1, \tau_2) = -\frac{i}{\hbar} \langle T_c u_i^R(\tau_1) u_j^L(\tau_2) \rangle = 0 \quad (17)$$

because there is no coupling term that would connect the left and right particles. The 1st-order term is

$$\begin{aligned} G_{ij,1}^{\text{RL}}(\tau_1, \tau_2) &= \left(-\frac{i}{\hbar} \right)^2 \sum_{mn} \int_c d\tau' V_{mn}^{\text{LR}}(\tau') \langle T_c u_m^L(\tau') u_n^R(\tau') u_i^R(\tau_1) u_j^L(\tau_2) \rangle, \\ &= \sum_{mn} \int_c d\tau' \left\{ -\frac{i}{\hbar} \langle T_c u_m^L(\tau') u_j^L(\tau_2) \rangle \right\} V_{mn}^{\text{LR}}(\tau') \left\{ -\frac{i}{\hbar} \langle T_c u_n^R(\tau') u_i^R(\tau_1) \rangle \right\}, \end{aligned} \quad (18)$$

where Wick's theorem is used to expand the four-particle average into two two-particle averages. There are actually three different ways to expand the four-particle average but the other two configurations vanish and we are left only with the term shown in the second equality. We would like to note that the use of Wick's theorem here is justified because the expansion is with respect to the quadratic H_0 .

Define the equilibrium Green's function of the free leads as

$$g_{ij}^\alpha(\tau_1, \tau_2) = -\frac{i}{\hbar} \langle T_c u_i^\alpha(\tau_1) u_j^\alpha(\tau_2) \rangle, \quad \alpha = \text{L, R}, \quad (19)$$

where the average is taken with respect to H_0 , i.e., the corresponding equilibrium distribution of the leads. Note that unlike the nonequilibrium G^{RL} , the equilibrium g^α

satisfies time-translation invariance and thus its Fourier transform exists and can be calculated. Writing Eq. (18) in terms of the equilibrium Green's functions we get

$$G_{ij,1}^{\text{RL}}(\tau_1, \tau_2) = \sum_{mn} \int_c d\tau' g_{in}^R(\tau_1, \tau') V_{nm}^{\text{LR}}(\tau') g_{mj}^L(\tau', \tau_2). \quad (20)$$

To get the lesser version of the nonequilibrium $G_{ij,1}^{\text{RL}}$ we employ analytic continuation and Langreth's theorem [14] to get

$$\begin{aligned} G_{ij,1}^{\text{RL},<}(t_1, t_2) &= \sum_{mn} \int_0^t dt' V_{nm}^{\text{LR}}(t') \\ &\times \left\{ g_{in}^{\text{R},r}(t_1, t') g_{mj}^{\text{L},<}(t', t_2) \right\} \end{aligned}$$

$$+ g_{in}^{R,<}(t_1, t') g_{mj}^{L,a}(t', t_2) \}, \quad (21)$$

where $g_{in}^{R,r}$ and $g_{mj}^{L,a}$ are the retarded and advanced versions of the equilibrium Green's functions, respectively. Similarly, the retarded and advanced versions of the first-order nonequilibrium Green's functions are

$$G_{ij,1}^{RL,\zeta} = \sum_{mn} \int_0^t dt' g_{in}^{R,\zeta}(t_1, t') V_{nm}^{RL}(t') g_{mj}^{L,\zeta}(t', t_2), \quad (22)$$

where $\zeta = r, a$. For the one-dimensional chain shown in Fig. 1 only the $i = 1$ and $j = 0$ label combination is nonzero. In addition, the coupling potential in Eq. (4) is nonzero only when $n = 1$ and $m = 0$ in the sum. All the other combinations of the indices do not contribute.

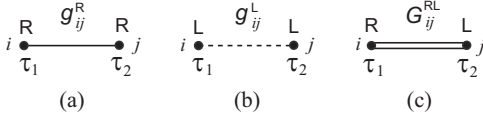


FIG. 3: Diagram representations for the equilibrium Green's functions (a) $g_{ij}^R(\tau_1, \tau_2)$ and (b) $g_{ij}^L(\tau_1, \tau_2)$, and (c) the nonequilibrium Green's function $G_{ij}^{RL}(\tau_1, \tau_2)$.

To facilitate the calculation of higher-order terms in the perturbation expansion we utilize a diagrammatic approach. Shown in Fig. 3 are the diagrams representing the relevant contour-ordered Green's functions in the expansion. A diagram can not be constructed for the zeroth-order term, Eq. (17), since it contains a u^L and a u^R pair. The first-order term, in contrast, has just the right number of double pairs of u^L and u^R and a V^{RL} to connect the two equilibrium Green's functions. The second-order term has the same shortcoming as the zeroth-order term, i.e., there is an extra u^L and u^R pair. In fact, all the rest of the even-ordered terms have the same extra u^L and u^R pair. All of the even-ordered terms therefore do not contribute to the perturbation expansion. As for the odd-ordered terms, they consist of repetitions of the first-order diagram. Shown in Fig. 4 is the perturbation expansion in diagram representation.

In the first equality of Fig. 4, the first and third-order terms are explicitly shown. Notice that the third-order term consists of two first-order terms. The diagram representation of the Dyson equation is shown in the second equality of Fig. 4. Note that this equation includes all terms in the expansion. Based on the diagrammatic rules, we can now write the Dyson equation for the nonequilibrium Green's function as

$$\begin{aligned} G_{ij}^{RL}(\tau_1, \tau_2) &= \sum_{mn} \int_c d\tau' g_{im}^R(\tau_1, \tau') V_{mn}^{RL}(\tau') g_{nj}^L(\tau', \tau_2) \\ &+ \sum_{mnpq} \int_c d\tau' \int_c d\tau'' g_{im}^R(\tau_1, \tau') V_{mn}^{RL}(\tau') g_{np}^L(\tau', \tau'') \\ &\times V_{pq}^{LR}(\tau'') G_{qj}^{RL}(\tau'', \tau_2). \end{aligned} \quad (23)$$

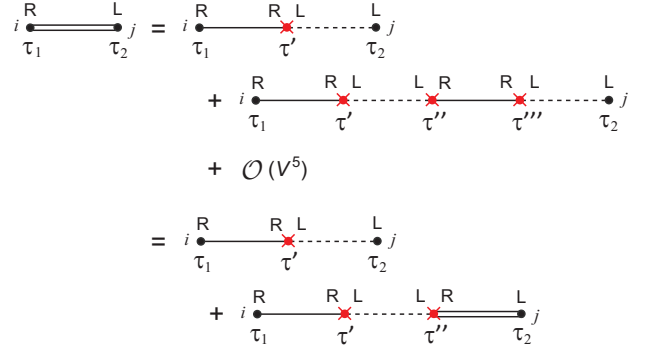


FIG. 4: (Color online) Diagrammatic perturbation expansion of G_{ij}^{RL} in terms of g^R and g^L . Each interaction vertex, i.e., the crossed-out dot (red online), includes an interaction potential V^{RL} and an integration with respect to the internal complex-time variable. The second equality is the diagram representation of the Dyson equation.

Applying Langreth's theorem [14] to Eq. (23) and then iterating the resulting equation, we get a closed-form formula that includes all orders of the expansion:

$$\begin{aligned} G_{ij}^{RL,<}(t_1, t_2) &= G_{ij,1}^{RL,<}(t_1, t_2) \\ &+ \sum_{mn} \int_0^t dt' G_{im}^{RL,r}(t_1, t') V_{mn}^{LR}(t') G_{nj,1}^{RL,<}(t', t_2) \\ &+ \sum_{mn} \int_0^t dt' G_{im,1}^{RL,<}(t_1, t') V_{mn}^{LR}(t') G_{nj}^{RL,a}(t', t_2) \\ &+ \sum_{mnpq} \int_0^t dt' \int_0^t dt'' G_{im}^{RL,r}(t_1, t') V_{mn}^{LR}(t') \\ &\times G_{np,1}^{RL,<}(t', t'') V_{pq}^{LR}(t'') G_{qj}^{RL,a}(t'', t_2). \end{aligned} \quad (24)$$

Equation (24) is the exact formula for the general nonequilibrium Green's function needed to calculate the current flowing through the left lead in Eq. (12). For the linear chain shown in Fig. 1, we use the coupling potential in Eq. (4) and the indices $i = n = q = 1$ and $j = m = p = 0$.

To solve Eq. (24) we need to determine $G_{ij,1}^{RL,<}$, $G_{ij}^{RL,a}$, and $G_{ij}^{RL,r}$. From Eq. (21) the first-order nonequilibrium Green's function can be calculated by

$$\begin{aligned} G_{10,1}^{RL,<}(t_1, t_2) &= - \int_0^t dt' k(t') \left\{ g_{11}^{R,r}(t_1, t') g_{00}^{L,<}(t', t_2) \right. \\ &\quad \left. + g_{11}^{R,<}(t_1, t') g_{00}^{L,a}(t', t_2) \right\}. \end{aligned} \quad (25)$$

To determine the full retarded Green's function we apply Langreth's theorem to Eq. (23) to get the equation

$$\begin{aligned} G_{10}^{RL,r}(t_1, t_2) &+ \int_0^t dt' k(t') G_{10,1}^{RL,r}(t_1, t') G_{10}^{RL,r}(t', t_2) \\ &= G_{10,1}^{RL,r}(t_1, t_2), \end{aligned} \quad (26)$$

where Eq. (22) is used for the first-order Green's functions. A similar equation can be derived for the full ad-

vanced Green's function. These two equations for the full retarded and advanced Green's functions can be solved by the process discussed in Sec. III.

III. NUMERICALLY CALCULATING THE ENERGY CURRENT

In the linear chain, the energy flowing out of the left lead, $I^L(t)$, at time t can be calculated using Eq. (13), the nonequilibrium lesser Green's function $G^{\text{RL},<}(t_1, t_2)$ shown in Eq. (24), and its derivative with respect to t_2 . From Eq. (24), the $G^{\text{RL},<}$ can be calculated from the first-order nonequilibrium lesser Green's function $G_1^{\text{RL},<}$, the full nonequilibrium retarded and advanced Green's functions, $G^{\text{RL},r}$ and $G^{\text{RL},a}$, respectively, and their derivatives with respect to t_2 . Furthermore, from Eq. (21), the $G_1^{\text{RL},<}$ can be calculated from the integral of equilibrium Green's functions $g^{\text{R},r}$, $g^{\text{L},<}$, $g^{\text{R},<}$, and $g^{\text{L},a}$. In addition, from Eq. (26), the full nonequilibrium retarded and advanced Green's functions can be calculated from the integral of equilibrium Green's functions. All of the nonequilibrium Green's functions, therefore, can be calculated from the integrals of equilibrium Green's functions. What we ultimately need then are the equilibrium Green's functions.

Equilibrium Green's functions satisfy time-translation invariance and therefore their Fourier transforms exist. In frequency space the retarded equilibrium Green's functions for the semi-infinite linear chain leads are known to be [15]

$$g_{ij}^{\alpha,r}[\omega] = -\frac{\lambda}{k} \lambda^{|i-j|}, \quad \alpha = \text{L, R}, \quad (27)$$

where the square brackets mean that the function is a Fourier transform and

$$\lambda = -\frac{\Omega}{2k} \pm \frac{1}{2k} \sqrt{\Omega^2 - 4k^2}, \quad (28)$$

where $\Omega = (\omega + i\eta)^2 - 2k - k_0$ and the choice between the plus or minus sign depends on satisfying $|\lambda| < 1$. Furthermore, the lesser equilibrium Green's function can be determined from [15]

$$g_{ij}^{\alpha,<}[\omega] = 2i f_\alpha \text{Im}\{g_{ij}^{\alpha,r}[\omega]\}, \quad (29)$$

where f_α is the Bose-Einstein distribution function of the α lead. Given a function $F[\omega]$ in frequency space its inverse Fourier transform is

$$F(t_1, t_2) = \int_{-\infty}^{\infty} \frac{d\omega}{2\pi} F[\omega] e^{-i\omega(t_1-t_2)}. \quad (30)$$

We can thus take the inverse Fourier transform of Eqs. (27) and (29) to determine the time-dependence of the corresponding equilibrium Green's functions. In addition, the advanced equilibrium Green's functions can be calculated from the retarded version by [9]

$$g_{ij}^{\alpha,a}[\omega] = (g_{ji}^{\alpha,r}[\omega])^*. \quad (31)$$

The integrals appearing in the inverse Fourier transforms are numerically calculated using the trapezoidal rule [16].

After numerically calculating the equilibrium Green's functions, we can use Eq. (25) to determine the first-order nonequilibrium lesser Green's function $G_{ij,1}^{\text{RL},<}$. We again use the trapezoidal rule to calculate the integral in Eq. (25).

To calculate the full nonequilibrium retarded Green's function $G_{ij}^{\text{RL},r}$, we solve Eq. (26). This equation is in the form of a Fredholm equation of the second kind [16]

$$f(t_a, t_b) + \int_0^t dt' f_1(t_a, t') k(t') f(t', t_b) = f_1(t_a, t_b), \quad (32)$$

where k and f_1 are assumed known and f is the unknown. To solve for f we discretize the time into N total intervals of incremental length $\Delta t = t/N$. Applying the trapezoidal rule to the integral in Eq. (26) we get

$$f(t_a, t_b) + \Delta t \cdot \left\{ \frac{1}{2} f_1(t_a, t_0) k(t_0) f(t_0, t_b) + \sum_{j=1}^{N-1} f_1(t_a, t_j) k(t_j) f(t_j, t_b) + \frac{1}{2} f_1(t_a, t_N) k(t_N) f(t_N, t_b) \right\} = f_1(t_a, t_b), \quad (33)$$

for a set of values of t_a and t_b . We can recast the calculation into a linear problem of the form

$$\begin{pmatrix} f(t_0, t_b) \\ f(t_1, t_b) \\ \vdots \\ f(t_N, t_b) \end{pmatrix} + \Delta t \cdot \begin{pmatrix} \frac{1}{2} f_1(t_0, t_0) k(t_0) & f_1(t_0, t_1) k(t_1) & \cdots & \frac{1}{2} f_1(t_0, t_N) k(t_N) \\ \frac{1}{2} f_1(t_1, t_0) k(t_0) & f_1(t_1, t_1) k(t_1) & \cdots & \frac{1}{2} f_1(t_1, t_N) k(t_N) \\ \vdots & \vdots & \ddots & \vdots \\ \frac{1}{2} f_1(t_N, t_0) k(t_0) & f_1(t_N, t_1) k(t_1) & \cdots & \frac{1}{2} f_1(t_N, t_N) k(t_N) \end{pmatrix} \begin{pmatrix} f(t_0, t_b) \\ f(t_1, t_b) \\ \vdots \\ f(t_N, t_b) \end{pmatrix} = \begin{pmatrix} f_1(t_0, t_b) \\ f_1(t_1, t_b) \\ \vdots \\ f_1(t_N, t_b) \end{pmatrix}. \quad (34)$$

We end up with a linear problem of the form

$$(\mathbf{1} + \mathbf{F}) \cdot \vec{f} = \vec{f}_1. \quad (35)$$

The unknown vector \vec{f} can be determined by decompos-

ing $(\mathbf{1} + \mathbf{F})$ using LU decomposition and then back substituting the result to the vector \vec{f}_1 . The $G_{10}^{\text{RL},r}(t_1, t_2)$ in Eq. (26) is numerically determined this way for values of t_1 and t_2 within the interval $[0, t]$. The same calculation can also be done to determine the advanced Green's function $G_{10}^{\text{RL},a}(t_1, t_2)$.

Having numerically calculated $G_{10,1}^{\text{RL},<}$, $G_{10}^{\text{RL},r}$, and $G_{10}^{\text{RL},a}$, we can then use Eq. (24) to determine $G_{10}^{\text{RL},<}(t_1, t_2)$ and its derivative with respect to t_2 . The current $I^L(t)$ is then calculated from Eq. (13). The same steps can be followed to calculate the energy current flowing out of the right lead, $I^R(t)$.

IV. NUMERICAL RESULTS

We numerically calculate the time-dependent behavior of the energy current flowing out of the leads. The coupling between the leads is harmonically modulated in the form

$$k(t) = \frac{k}{2}(1 - \cos \omega_d t), \quad (36)$$

where ω_d is the driving frequency. Note that this modulated coupling has the same order as k and thus, a perturbative calculation is not expected to produce accurate results. In contrast to perturbative calculations, we calculate the current exactly by numerically solving the Dyson equation. In all of our calculations, we set the interparticle coupling $k = 0.625 \text{ eV}/(\text{\AA}^2 \text{ u})$ and the on-site spring constant $k_0 = 0.0625 \text{ eV}/(\text{\AA}^2 \text{ u})$. These choices lead to a natural time scale that we also use as the unit of time, $[t] = 10^{-14} \text{ s}$. We use a time increment of $\Delta t = 0.1 [t]$ in our calculations.

We explore several variations of our setup. First, we study the energy current when there is no thermal bias between the leads. Let the temperature of the leads be $T = T_L = T_R$. Shown in Fig. 5 is the time-dependent behavior of the current flowing out of the left lead for four different driving frequencies and three different lead temperatures. Notice that the current does not exactly follow the modulation. If we look at the corresponding Fourier transforms of the current, $I^L[\omega]$, we find three peaks at three specific frequencies in the frequency space and zero everywhere else. The strongest peak has frequency that corresponds to the driving frequency ω_d . The two smaller peaks have frequencies that are twice and three times the driving frequency. The current is thus a combination of three waves. This is also evident in Fig. 5 where we find three peaks, and therefore three waves, for every peak in the modulation.

Although the amplitude of the modulated coupling is kept constant at $k/2$, as the driving frequency is increased the peaks in the current also increases. In addition, as the driving frequency becomes sufficiently high, transient behavior in the current becomes visible. Transient behavior becomes pronounced when the modulation of the

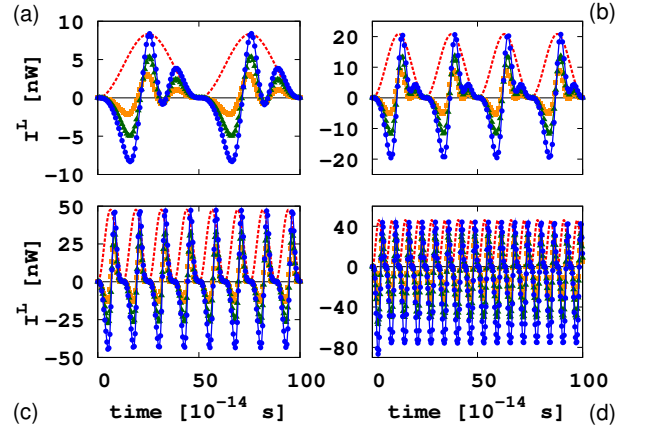


FIG. 5: (Color online) The current $I^L(t)$ as a function of time when the driving frequency is (a) $\omega_d = 0.125 [1/t]$, (b) $\omega_d = 0.25 [1/t]$, (c) $\omega_d = 0.5 [1/t]$, and (d) $\omega_d = 1 [1/t]$. The leads have the same temperatures $T = T_L = T_R$ with values $T = 10 \text{ K}$ (■, orange online), $T = 300 \text{ K}$ (▲, green online), and $T = 500 \text{ K}$ (●, blue online). The harmonic modulation of the coupling is shown (dashed line, red online) as a guide. Its amplitude is not drawn to scale.

coupling changes rapidly. We look at transient behavior more closely in Fig. 9.

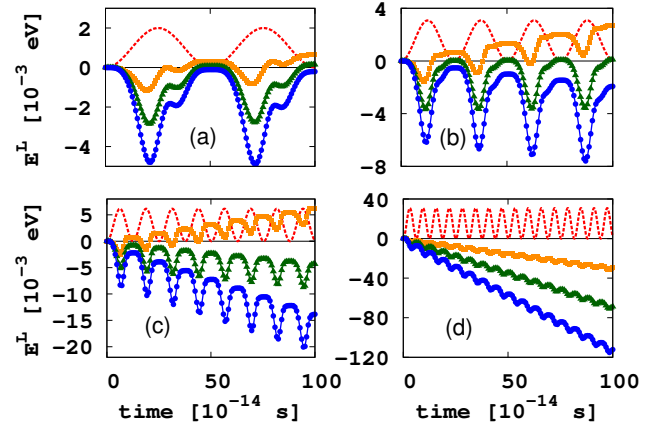


FIG. 6: (Color online) The energy $E^L(t)$ as a function of time for driving frequencies (a) $\omega_d = 0.125 [1/t]$, (b) $\omega_d = 0.25 [1/t]$, (c) $\omega_d = 0.5 [1/t]$, and (d) $\omega_d = 1 [1/t]$. The leads have the same temperature $T = T_L = T_R$ with values $T = 10 \text{ K}$ (■, orange online), $T = 300 \text{ K}$ (▲, green online), and $T = 500 \text{ K}$ (●, blue online). The harmonic modulation of the coupling is shown (dashed line, red online) as a guide. Its amplitude is not drawn to scale.

In Fig. 5, we notice that the current appears to be more on the negative axis as the driving frequency is increased. Since we define the left current in Eq. (6) as the energy flowing out of the left lead, a negative value means that the energy is flowing into the lead. To be more definite, we calculate how much energy has flowed into the left

lead by

$$E^L(t) = \int_0^t I^L(t') dt'. \quad (37)$$

We again use the trapezoidal rule to numerically calculate the integral. Shown in Fig. 6 is the energy $E^L(t)$ for the four different driving frequencies and three different temperatures corresponding to those shown in Fig. 5. Notice that for the highest driving frequency, as shown in Fig. 6(d), the energy increases negatively in time for all three temperatures shown. Therefore, harmonically modulating the lead coupling by a driving frequency of $\omega_d = 1$ [1/t] moves energy from the external agent into the left lead. Furthermore, since there is no thermal bias between the leads, the left and right leads are indistinguishable. The plots for $I^R(t)$ and $E^R(t)$ are therefore exactly the same as those shown for the left lead in Fig. 5 and Fig. 6, respectively. The external agent therefore supplies energy to both the left and right leads.

Decreasing the driving frequency, we see from Fig. 6 that for certain values of the temperature, instead of the energy flowing into the leads, energy is actually flowing out from the leads. In Fig. 6(c), for example, when the driving frequency is $\omega_d = 0.5$ [1/t], energy flows into the leads when $T = 300$ K and $T = 500$ K but it flows out of the leads when $T = 10$ K.

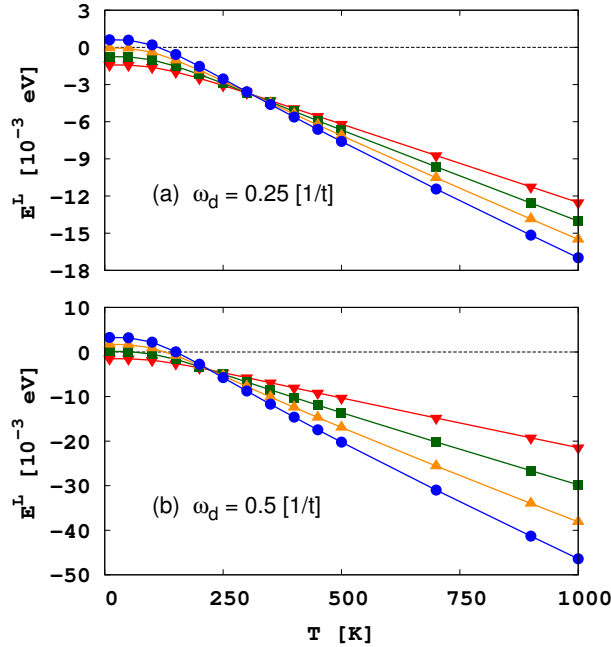


FIG. 7: The energy E^L as a function of the lead temperature T , which is the same for both leads. Each curve in the plot corresponds to a specific value of time. (a) For $\omega = 0.25$ [1/t] at time $t = 11.8$ [t] (∇ , red online), $t = 36.9$ [t] (\blacksquare , green online), $t = 62.1$ [t] (\blacktriangle , orange online), and $t = 87.2$ [t] (\bullet , blue online). (b) For $\omega = 0.5$ [1/t] at time $t = 19.4$ [t] (∇ , red online), $t = 44.6$ [t] (\blacksquare , green online), $t = 69.7$ [t] (\blacktriangle , orange online), and $t = 94.8$ [t] (\bullet , blue online).

Shown in Fig. 7 are plots of how E^L varies for different values of the driving frequency and lead temperature, at specific instants of time. Note that in Fig. 6 the energy E^L oscillates in time. The data points in Fig. 7 are chosen from Fig. 6 during the times when E^L is at a trough in the oscillating energy. We can also choose different sets of data points, e.g., points at the crest instead of the trough, and then plot them like those in Fig. 7. The plots, however, will look the same except for a translation along the vertical axis.

In Fig. 7, the E^L values are negative at higher temperatures. At lower temperatures, however, E^L can be positive, depending on the values of ω_d and t . Notice that there is a temperature T_c where the curves, for one value of ω_d , intersect. In Fig. 7(a), for example, $T_c \approx 300$ K. This T_c is lower for higher ω_d values, as shown in Fig. 7(b). Now, since the choice of taking data points only at the trough of E^L is arbitrary, we may also choose a different location along E^L such that at T_c we get $E^L(T_c) = 0$, for any time t . For such a choice, the values of E^L below T_c are positive and above T_c are negative.

Notice in Fig. 7 that the slope of the curves becomes steeper at later times. The value of E^L at $T = T_c$, however, remains the same at any time t . Therefore, at much later times when the slope of the curves are much steeper, when $T > T_c$ both the left and right leads absorb energy from the external agent, while when $T < T_c$ the leads emit energy to the external agent.

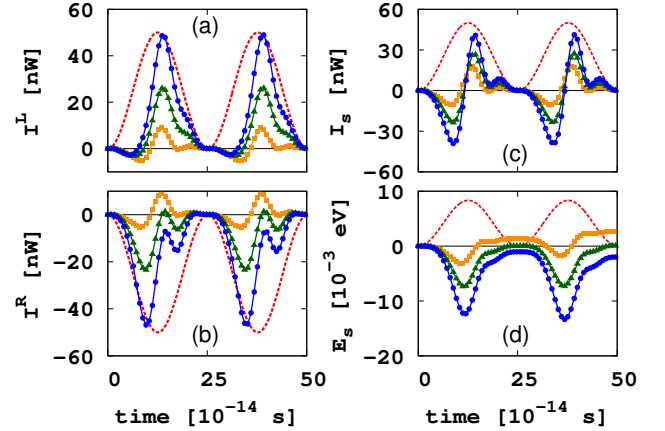


FIG. 8: (Color online) Time evolution of (a) the current in the left lead, I^L , and (b) the right lead, I^R , (c) the sum of the currents, $I_s = I^L + I^R$, and (d) the sum of the energies in both leads, E_s . The average temperature between the leads are $T_{\text{ave}} = 10$ K (\blacksquare , orange online), $T_{\text{ave}} = 300$ K (\blacktriangle , green online), and $T_{\text{ave}} = 500$ K (\bullet , blue online). The driving frequency $\omega_d = 0.25$ [1/t]. The harmonic modulation of the coupling is shown (dashed line, red online) as a guide. Its amplitude is not drawn to scale.

We now consider what happens when the leads have

different temperatures. Let the lead temperatures be

$$\begin{aligned} T_L &= (1 + \varepsilon) T_{\text{ave}}, \\ T_R &= (1 - \varepsilon) T_{\text{ave}}, \end{aligned} \quad (38)$$

i.e., the left lead is warmer than the right lead. Heat would therefore spontaneously flow, except for transient effects, from the left lead to the right lead if the coupling between the leads is not modulated in time [10]. In our calculations we consider a temperature variation of $\varepsilon = 0.1$. Figure 8(a) shows the current flowing out of the left lead as a function of time when the driving frequency $\omega_d = 0.25$ [1/t]. The time evolution of the current does not exactly follow the modulation of the lead coupling. Taking the Fourier transform of the current produces three peaks at frequencies ω_d , $2\omega_d$, and $3\omega_d$. This situation is similar to the case when the leads have the same temperature. Notice in Fig. 8(a) that the current is mostly positive and thus, as expected, energy is flowing out of the warmer left lead. Shown in Fig. 8(b) is the current flowing out of the right lead. For the cooler right lead, the question of whether the current is mostly negative or positive depends on the temperature of the lead. When $T_{\text{ave}} = 10$ K, the current is mostly positive and therefore, energy is mostly flowing out of the cooler right lead. At $T_{\text{ave}} = 10$ K therefore, the current is flowing out of both the left and right leads, i.e., energy from both leads is being absorbed by the external agent. In contrast, when $T_{\text{ave}} = 500$ K the current in the right lead is mostly negative and therefore energy is mostly flowing into the cooler right lead.

Notice that the plots in Fig. 8(b) are not mirror reflections, with respect to the horizontal axis, of the plots in Fig. 8(a). When the sum of the currents are taken, i.e., $I_s(t) = I^L(t) + I^R(t)$, the results are the plots shown in Fig. 8(c). Note that although the plots only show the time evolution of I_s up to time $t = 50$ [t] our calculations extend until time $t = 100$ [t]. Comparing Fig. 8(c) to Fig. 5(b), we find the plots to coincide (note that the plot in Fig. 5(b) is only for the left lead and so the values of the current should be multiplied by two). Furthermore, we find that the values of $I_s(t)$ when $\varepsilon = 0.1$ are numerically very close to, if not the same as, the values of $I_s(t)$ when $\varepsilon = 0$ at each corresponding instant of time t . Our numerical results thus hint that the sum of currents $I_s(t)$ may be independent of the value of ε .

Modulating the lead coupling when $\varepsilon = 0.1$ therefore results in plots of the net current I_s that numerically coincide with those when $\varepsilon = 0$. The direction of the current flow in each lead, however, differs depending on whether the leads have the same or different temperatures. When the leads have the same temperature the current can either flow into both of the leads at the same time or flow out of the leads at the same time. In contrast, when the leads have different temperatures, the energy can flow out of both the warmer left lead and the cooler right lead resulting in a net current that flows out of the linear chain system and into the external agent. This happens, for example, when $T_{\text{ave}} = 10$ K in Fig. 8.

Increasing the average temperature to $T_{\text{ave}} = 300$ K, we find a balance between the energy that flows out of the warmer left lead and the energy that flows into the cooler right lead resulting in no net energy flow for the whole system, as shown in Fig. 8(d). Increasing the average temperature further to $T_{\text{ave}} = 500$ K, we find that energy flows out of the left lead and flows into the cooler right lead resulting in a net energy flowing into the chain system. We thus see that the current can either flow into or out of the cooler right lead depending on the value of the average temperature of the leads.

The driving frequency in Fig. 8 is $\omega_d = 0.25$ [1/t]. As shown in Fig. 7 there is a temperature T_c where there is no net energy flowing into or out of the linear chain system. When ω_d is varied the T_c also varies. Similarly, for the case when one of the leads is warmer than the other, when $T_{\text{ave}} < T_c$ we find that the current flows out of the cooler right lead resulting in a net energy flowing out of the chain system. When $T_{\text{ave}} > T_c$ we find the current to flow into the cooler right lead resulting in a net energy flowing into the chain system. Note that for any value of T_{ave} energy flows out of the warmer left lead.

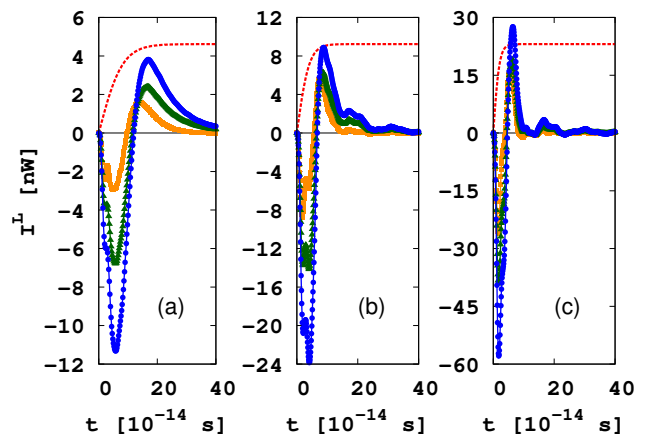


FIG. 9: (Color online) The current $I^L(t)$ as a function of time t when the coupling between the leads is gradually increased with driving frequencies (a) $\omega_d = 0.125$ [1/t], (b) $\omega_d = 0.25$ [1/t], and (c) $\omega_d = 0.5$ [1/t]. Both leads have the same temperature $T = 10$ K (■, orange online), $T = 300$ K (▲, green online), and $T = 500$ K (●, blue online). The gradually increasing coupling is shown (dashed line, red online) as a guide. Its amplitude is not drawn to scale.

We now investigate the effects of the speed of modulation on the transient behavior of the current. In Fig. 5 we find that the transient becomes visible as the driving frequency ω_d is increased. To clearly see the effects of how fast the coupling is changing, we consider gradually increasing the coupling in the form

$$k(t) = k \tanh \omega_d t. \quad (39)$$

Shown in Fig. 9 are plots of the energy current in time for various values of the driving frequency ω_d and temperature T . We consider the leads to have the same temper-

ature T and thus, for later times, we expect there to be no steady-state current. In Fig. 9 we see that at earlier times the transient behavior shows up as rapid bumps in the current and then eventually subsides down to zero at later times. The amplitude of the transient current depends on the values of the driving frequency ω_d and the temperature T of the leads. The faster ω_d and higher T produce larger transient current amplitudes.

V. SUMMARY

Dynamically modulating the coupling between the leads in the form shown in Eq. (36) can result in the energy current to either flow into or out of the leads, depending on the values of the driving frequency ω_d and the lead temperature T , even when the leads have the same temperature. For such a case, it is possible for the energy current to either flow out of both leads at the same time or flow into both leads at the same time, as shown in Fig. 6. In addition, in Fig. 7 we see that for a given value of ω_d there exists a temperature T_c where, in the long-time limit, when the temperature of the leads $T < T_c$ we find the current to flow out of both leads and when $T > T_c$ we find the current to flow into both

leads. For the case when the leads have different temperatures, with $\varepsilon = 0.1$, the direction of the flow of the energy current in the cooler lead depends on the values of T_{ave} and ω_d . When $T_{\text{ave}} < T_c$ the current flows out of the cooler lead but when $T_{\text{ave}} > T_c$ the current flows into the cooler lead. Current flows out of the warmer lead for any temperature T_{ave} . Gradually increasing the lead coupling in the form shown in Eq. (39) shows that the amplitude of the transient depends on how fast the lead coupling changes. Faster changes in the lead coupling result in larger transient amplitudes, as shown in Fig. 9. As a consequence, harmonically modulating the lead coupling with a faster driving frequency results in a more pronounced transient behavior in the current, as shown in Fig. 5.

Acknowledgments

We would like to thank José García-Palacios, Lifa Zhang, Jin-Wu Jiang, Meng Lee Leek, Xiaoxi Ni, Bijay Agarwalla, and Juzar Thingna for insightful discussions. This work is supported in part by an NUS research grant number R-144-000-257-112.

-
- [1] Z. Huang, B. Xu, Y. Chen, M. Di Ventra, and N. Tao, *Nano Lett.* **6**, 1240 (2006); M. Tsutsui, M. Taniguchi, and T. Kawai, *ibid.* **8**, 3293 (2008); Z. Huang, F. Chen, R. D'Agosta, P.A. Bennett, M. Di Ventra, and N. Tao, *Nat. Nanotechnol.* **2**, 698 (2007).
 - [2] C. Van den Broeck and R. Kawai, *Phys. Rev. Lett.* **96**, 210601 (2006); M. van den Broek and C. Van den Broeck, *ibid.* **100**, 130601 (2008).
 - [3] B.-Q. Ai, D. He, and B. Hu, *Phys. Rev. E* **81**, 031124 (2010).
 - [4] D. Segal, *Phys. Rev. Lett.* **101**, 260601 (2008); D. Segal and A. Nitzan, *Phys. Rev. E* **73**, 026109 (2006); D. Segal, *J. Chem. Phys.* **130**, 134510 (2009).
 - [5] N. Nakagawa and T.S. Komatsu, *Europhys. Lett.* **75**, 22 (2006).
 - [6] F. Zhan, N. Li, S. Kohler, and P. Hänggi, *Phys. Rev. E* **80**, 061115 (2009); N. Li, F. Zhan, P. Hänggi, and B. Li, *ibid.* **80**, 011125 (2009).
 - [7] J. Ren and B. Li, *Phys. Rev. E* **81**, 021111 (2010).
 - [8] M. Rey, M. Strass, S. Kohler, P. Hänggi, and F. Sols, *Phys. Rev. B* **76**, 085337 (2007); L. Arrachea, M. Moskalets, and L. Martin-Moreno, *ibid.* **75**, 245420 (2007); M. Moskalets and M. Büttiker, *ibid.* **70**, 245305 (2004); Y. Wei, L. Wan, B. Wang, and J. Wang, *ibid.* **70**, 045418 (2004); B. Wang and J. Wang, *ibid.* **66**, 125310 (2002); M. Moskalets and M. Büttiker, *ibid.* **66**, 205320 (2002).
 - [9] See, for a review, J.-S. Wang, J. Wang, and J.T. Lü, *Eur. Phys. J. B* **62**, 381 (2008).
 - [10] E.C. Cuansing and J.-S. Wang, *Phys. Rev. B* **81**, 052302 (2010).
 - [11] J. Schwinger, *J. Math. Phys.* **2**, 407 (1961); L.V. Keldysh, *Sov. Phys. JETP-USSR* **20**, 1018 (1965).
 - [12] See, for a review, J. Rammer and H. Smith, *Rev. Mod. Phys.* **58**, 323 (1986).
 - [13] A.-P. Jauho, N.S. Wingreen, and Y. Meir, *Phys. Rev. B* **50**, 5528 (1994).
 - [14] See, for example, H. Haug and A.-P. Jauho, *Quantum Kinetics in Transport and Optics of Semiconductors*, 2nd ed. (Springer, New York, 2008).
 - [15] J.-S. Wang, N. Zeng, J. Wang, and C.K. Gan, *Phys. Rev. E* **75**, 061128 (2007).
 - [16] W.H. Press, S.A. Teukolsky, W.T. Vetterling, and B.P. Flannery, *Numerical Recipes: The Art of Scientific Computing*, 3rd ed. (Cambridge, New York, 2007).